JOURNAL OF GEOPHYSICAL RESEARCH, VOL. 103, NO. D8, PAGES 8909–8917, APRIL 27, 1998

Equatorial diurnal variations observed in UARS Microwave Limb Sounder temperature during 1991–1994 and simulated by the Canadian Middle Atmosphere Model

D. L. Wu
Jet Propulsion Laboratory, California Institute of Technology, Pasadena, California

C. McLandress
Department of Atmospheric Science, University of Washington, Seattle

W. G. Read, J. W. Waters, and L. Froidevaux
Jet Propulsion Laboratory, California Institute of Technology, Pasadena, California

Abstract. This paper presents a study of the equatorial diurnal tide at 27–55 km based on temperature data from the Upper Atmosphere Research Satellite (UARS) Microwave Limb Sounder (MLS). The MLS temperature retrieval is significantly improved in the lower stratosphere with the recent (version 4) software and able to provide useful tidal information down to 22 hPa. The diurnal amplitude and phase, derived from MLS ascending-descending temperature differences, show a strong annual variation in the lower stratosphere and a semiannual variation in the upper stratosphere and mesosphere, which are in good agreement with other UARS measurements and simulations from the Canadian Middle Atmosphere Model (CMAM). The largest differences between the observation and the model appear at 22 and 1 hPa, reflecting some shortcomings in current tidal modeling. It is shown in MLS observations that the (1,1) tide suffers severe reduction in amplitude at 1 hPa which could be caused by the interference between the propagating tide and the component generated by stratospheric ozone heating. The data also indicate the possible presence of a short-lived propagating component (i.e., the (1, 2) mode) in the lower stratosphere, which can be excited in the upper troposphere but damped quickly as it propagates upward.

1. Introduction

The middle-atmospheric diurnal tide is generated mainly by two heating sources (H_2O and O_3) that are distributed in the upper troposphere and stratosphere [*Chapman and Lindzen*, 1970; *Forbes and Garrett*, 1979]. These diurnal forcings excite various modes in terms of classical tidal theory that either propagate or are trapped vertically in the atmosphere. The predominant propagating component of the diurnal tide, known as the symmetric (1,1) mode with a vertical wavelength of ~30 km, plays an important role in the mesosphere and lower thermosphere where it breaks and deposits momentum and energy. The trapped components are restricted vertically to their source altitudes and dissipate/redistribute forcing energy locally. The tidal structure in the real atmosphere may depart remarkably from the description of classical tidal theory as it interacts with the background atmosphere. For example, the symmetric (1,1) tide is shown to be distorted at solstice when the mean flow is very asymmetric about the equator [*Vial*, 1986; *Vincent et al.*, 1989]. In addition, other interactions, such as tidal/gravity wave and tidal/planetary wave, are also thought to contribute considerably to tidal variability [*Lindzen*, 1981; *Walterscheid*, 1981; *Fritts and Vincent*, 1987; *Vial et al.*, 1991].

Recent satellite observations reveal various scales of tidal variability in the middle and upper atmosphere [e.g., *Hitchman and Leovy*, 1985; *Hays and Wu*, 1994; *McLandress et al.*, 1996]. The long-term tidal variability includes semiannual, annual, and biennial modulations in the diurnal tidal amplitude and phase [*Burrage et al.*, 1995]. It has been shown that longitudinal variations can be as large as 50% of the migrating tide and latitudinal structures can depart largely from the Hough mode solutions [*Wu et al.*, 1996]. These new observations provide complementary pictures of the tidal structures that have not previously been seen from ground-based sensors and stimulate the need for a better understanding of tidal variations [e.g., *Reed et al.*, 1969; *Manson et al.*, 1985; *Vincent et al.*, 1989].

To further investigate the diurnal tidal variability, we analyze the temperature data from the Upper Atmosphere Research Satellite Microwave Limb Sounder (UARS MLS), which cover altitudes of 28–55 km and compare them against the tidal simulations from the three-dimensional Canadian Middle Atmosphere Model (CMAM). In earlier studies with UARS data, the diurnal tide is analyzed mostly in the mesosphere and lower thermosphere where its wind amplitudes are large [*Hays and Wu*, 1994; *Burrage et al.*, 1995; *McLandress et al.*, 1996]. It is difficult to obtain tidal information in the stratosphere from wind fields due to much smaller tidal amplitudes. Therefore the MLS temperature broadens the altitude range of UARS study of the diurnal tide, providing further insights on the tidal variability. On the other hand, the long-term variation of the diurnal tide is not simulated or not done very well

Paper number 98JD00530.
0148-0227/98/98JD-00530$09.00

Table 1. MLS NCEP Differences for MLS Version 3 Temperature

Pressure, hPa	Bias, K		Scaling (NCEP/MLS)		s.d., K	
	South	North	South	North	South	North
0.46	−2.1	0.5	0.350	0.250	10.5	12.0
1.0	4.2	1.6	0.601	0.583	7.1	8.2
2.2	0.0	−2.3	0.683	0.675	6.3	7.6
4.6	−4.5	−4.7	0.641	0.728	6.8	6.9
10	−4.8	2.3	0.864	0.940	4.2	4.0
22	−5.1	−1.5	0.730	0.695	6.6	6.1

by many tidal models due to the yet poor understanding of the tidal variability. The CMAM, a nonlinear general circulation model spanning the altitude range 0–100 km, is able to reproduce some realistic tides in the middle atmosphere by incorporating important processes of tidal generation and propagation. Here we present a multiyear climatology of the diurnal tide observed by MLS and discuss the comparisons with the CMAM.

2. Temperature Measurement

The UARS MLS measures pressure, temperature, and molecular abundance in the middle atmosphere from emission features near 63, 183, and 205 GHz [*Waters*, 1993; *Barath et al.*, 1993]. Temperature is retrieved on constant pressure surfaces ranging from 46 to 0.46 hPa, based on radiance profiles of O_2 emission lines around 63 GHz [*Fishbein et al.*, 1996]. MLS resolves the O_2 lines at each tangent point with 15 spectral channels so that tangent pressure and temperature can be retrieved simultaneously. When there is little or no temperature sensitivity, MLS temperature is gradually constrained to the COSPAR International Reference Atmosphere (CIRA) climatology [*Fleming et al.*, 1988] (at higher altitudes) and the National Center for Environmental Predictions (NCEP) temperature (at lower altitudes).

In normal operation the MLS instrument step scans the atmospheric limb in ~65 from 90 km to the surface in increments of ~5 km in the mesosphere and 1–3 km in the stratosphere and troposphere. The MLS always views 90° from the flight direction on the shaded side of the satellite to stay away from direct sunlight. The MLS tangent point track yields a latitudinal coverage from 34° in one hemisphere to 80° in the other due to the 57° orbital inclination angle. There are 15 orbits each day slowly precessing westward (~5° per day at the equator) to produce measurements that differ slightly in local time (by ~20 min) each day. In ~36 days a complete diurnal cycle can be sampled, and one can resolve the mean, diurnal, and semidiurnal components in the equatorial regions if the tides are stationary over the period. In addition, the satellite makes 10 yaw maneuvers each year allowing alternate views of the two polar regions.

For the tidal analysis we use MLS version 4 (V4) temperatures at 22–0.46 hPa that are thought to have a significant improvement at 22 hPa over previous versions in terms of systematic error reduction. The temperature at 46 hPa is noisier than at other levels and is not used for the tidal analysis since some systematic errors have not been completely understood. We will briefly discuss here the features and quality of the MLS V4 temperature data.

2.1. MLS V4 Temperature

MLS V4 temperature is retrieved at altitudes above ~20 km, but useful data are limited to 22, 10, 4.6, 2.2, 1.0, and 0.46 hPa pressure levels. Several changes made in the MLS V4 algorithm have helped improve the temperature retrieval, including better estimates for O_2 line parameter values, radiometer sideband ratios, a priori errors, and the addition of 46-hPa temperature retrieval. Further details about MLS temperature-pressure retrievals can be found in the version 3 (V3) temperature validation [*Fishbein et al.*, 1996]. Here we focus on the differences between the V4 and V3 temperature products and the method to extract the tidal information from the data.

MLS V4 temperature is expected to have a smaller systematic error and less constraint from NCEP and climatological temperatures than the V3 product. The V3 temperature exhibits a large (2 K peak-to-peak) systematic error at 22 hPa between ascending and descending measurements that synchronizes with the UARS yaw cycle. One can readily recognize the error in a time series of temperature differences between ascending and descending measurements, which shows an unrealistic discontinuity before and after the UARS yaw maneuvers. Since the yaw cycle is aliased to local time sampling and the induced error is greater than or comparable to the tidal amplitude, such a systematic effect is unacceptable to the tidal analysis.

To further validate MLS temperature, we compare the data of the two versions against NCEP temperature, which helps better understand the quality of both MLS and NCEP temperatures. NCEP temperature is tied closely to the data quality of original sources, namely, radiosondes in the northern hemisphere (NH) and NOAA Tiros Operational Vertical Sounder (TOVS) in the southern hemisphere (SH). Because radiosonde measurements are more reliable in the lower stratosphere and troposphere than TOVS, it is important to recognize that the quality of NCEP temperature may vary significantly with place and height.

2.2. Measurement Errors

For MLS-NCEP temperature comparisons, we carry out separate analyses for the southern and northern hemispheres and restrict the observations to the high-latitude winter (40° poleward) where temperature variability is high in the stratosphere. Two winter periods are selected to cover both SH and NH, and each ensemble contains about 2 months worth of data or 30,000 profiles.

The MLS-NCEP temperature differences are summarized in Tables 1–2 with the following statistical variables: (1) bias, the mean difference between the two data sets; (2) scaling, the

Table 2. MLS NCEP Differences for MLS Version 4 Temperature

Pressure hPa	Bias, K		Scaling (NCEP/MLS)		s.d., K	
	South	North	South	North	South	North
0.46	2.8	0.2	0.304	0.181	12.0	14.0
1.0	8.2	6.5	0.578	0.565	7.6	8.8
2.2	1.1	−1.5	0.692	0.682	6.2	7.5
4.6	−0.1	−0.3	0.677	0.744	6.1	6.4
10	−3.3	−1.1	0.760	0.828	5.5	5.3
22	−3.7	0.2	0.849	0.850	4.8	4.0
46	4.2	3.5	0.810	0.669	5.7	6.6

slope of the best fit linear relationship; and (3) standard deviation of the difference, which measures the total MLS temperature precision and the atmospheric variability sometimes not being captured by NCEP. The NCEP temperature used for the comparison is the analysis at 1200 UT only. Therefore local time variability may contribute to the standard deviation of MLS-NCEP differences.

Improvements from MLS V3 to V4 can be seen in the reduction of the MLS(V4)-NCEP bias at 22.0–2.0 hPa. Especially at 22 hPa, the better agreement is needed for MLS because NCEP temperature is thought to have better quality at lower altitudes. Both versions of MLS data indicate the NCEP-MLS differences are ~4 K worse in the SH than in the NH at 10 and 22 hPa. It could be due to lack of radiosonde measurements in the SH. Moreover, in a comparison of NCEP and U.K. Meteorological Office (UKMO) temperatures, *Manney et al.* [1996] found that the NCEP temperature in the southern winter tends to be warmer in the lower stratosphere but agrees better with UKMO in the northern winter, implying that MLS V4 temperature would agree better overall with the UKMO temperature.

Nevertheless, there is a concern about the MLS temperature retrievals at 1 and 0.46 hPa which might produce a temperature lapse rate too steep in the mesosphere when compared to NCEP. This is noticeable in the NCEP-MLS differences at 1 and 0.46 hPa where the bias starts to oscillate between the MLS retrieval surfaces (a positive bias at 22 hPa is not shown), which can be caused by poor sensitivity and loose constraint on the a priori temperature in the retrieval. Especially at 0.22 and 0.46 hPa, where MLS temperature sensitivity is decreasing rapidly, the temperature lapse rate sometimes is overestimated. On the other hand, the NCEP temperature is smoothed over a broader altitude range as it approaches the assimilation upper boundary. Therefore it is not anticipated that MLS temperature should agree well with NCEP temperature at these levels but the comparison helps identify the noise-induced retrieval instability. For similar reasons, the poorer temperature sensitivity can also affect MLS 46-hPa temperature quality. Since the error is much greater than the expected tidal amplitude, we omit the tidal analysis at this level.

A scaling error can be caused by different temperature sensitivities or vertical/horizontal resolutions between the MLS and NCEP products. The vertical resolution of MLS temperature is ~5 km; this resolution is better than that from TOVS which the NCEP analysis depends on mostly in the upper stratosphere. Since the upper boundary of NCEP analysis is at 0.4 hPa, weaker temperature sensitivity in the NCEP analysis may be attributed to the decreasing NCEP/MLS ratios with height. It can be seen that the MLS (V4) temperature is less reliable at 46 hPa than NCEP as the NCEP/MLS ratio drops substantially to 0.67 from 0.85 at 22 hPa in the NH. The scaling differences also suggest an improvement made with MLS (V4) algorithms for 22-hPa temperature by adding the temperature retrieval at 46 hPa. The numbers at 22 hPa increase from 0.73(0.70) in the SH(NH) to 0.85(0.85), providing useful information on the tidal and other wave studies.

3. Data Sampling and Analysis

MLS measured temperature on a regular basis during September 1991 to October 1994 with twice-daily sampling at equatorial latitudes. To assure the sampling of two distinct local times, the tidal analysis is restricted to latitudes less than 25° so that reliable and continuous results can be obtained regardless of the spacecraft's yaw situations. Since we are to derive both diurnal and semidiurnal amplitudes and phases, a wide range of local time coverage is needed so that they can be distinguishable from the mean component. When the local times of ascending-descending orbits are too close together at the turning latitudes, severe aliasing can occur between the tides and the mean or slowly moving planetary waves.

The worse case in our analysis is at 25° latitude where the local time difference between ascending and descending orbits is 5 hours, and it becomes 10 hours after the spacecraft is yawed to view the other hemisphere. We have studied potential aliasing problems associated with these sampling patterns and found that, with the assumption that the tides are relatively stationary over the fitting period, the 5-hour A–D difference and the local time coverage due to the orbital precession will provide enough information to extract the mean tidal information. One can also verify the tidal information derived at this latitude by comparing the amplitude before and after the satellite yaw maneuver since the tidal amplitude variations should be independent of the sampling changes. A sudden amplitude change due to sampling modifications often indicates a strong aliasing associated with the information desired.

For the analysis procedure, we first compute daily longitudinal averages for separate ascending (A) and descending (D) orbits at every 5° latitude bin. Such temperature averages help remove most of the longitudinal variability likely due to planetary waves and nonmigrating tides. The local times sampled at these nodes for a given latitude are nearly constant for all the longitudes within a day. Having obtained the ascending and descending averages at each latitude, we then remove the mean component by taking the difference. Similarly, we obtain A–D differences for the local time at these nodes. These A–D temperature differences and associated local times preserve all the information for the migrating tides and go into the fitting of the diurnal and semidiurnal amplitudes and phases. It is necessary to remove the mean component on a daily basis rather than on a monthly timescale because mean temperature can vary rapidly sometimes, causing a larger uncertainty in the tidal amplitude obtained. For example, the rate of temperature change is 0.25 K/d at 10 hPa during January and February.

Figure 1 gives an example of the temperature A–D difference at the equator and the local time variation of the ascending node. The local time variation on the descending node is similar to one shown in Figure 1, both drifting slowly with time as a result of the orbital precession. The local time difference between ascending and descending nodes remains constant within the UARS month but is latitude-dependent. Because of the local time drift of these sampling nodes, the diurnal tide will manifest itself as an oscillation in the time series of the A–D difference that has the same period as the orbital precession (~72 days). Superimposed on the 72-day oscillation is the seasonal modulation of the amplitude of the diurnal tide. The tidal phase variation and amplitude growth with respect to height are clearly evident in the A–D temperature differences.

We obtain the time series of the tidal amplitudes and phases by fitting the diurnal and semidiurnal harmonics to the A–D temperature differences in a 100-day running window. This window size is chosen to reduce remaining systematic noise as much as possible but retain seasonal and longer-term tidal variability. Although the systematic error is significantly reduced in the V4 retrieval, there may still exist a bias of ~0.3 K between the ascending-descending sequences. This bias could

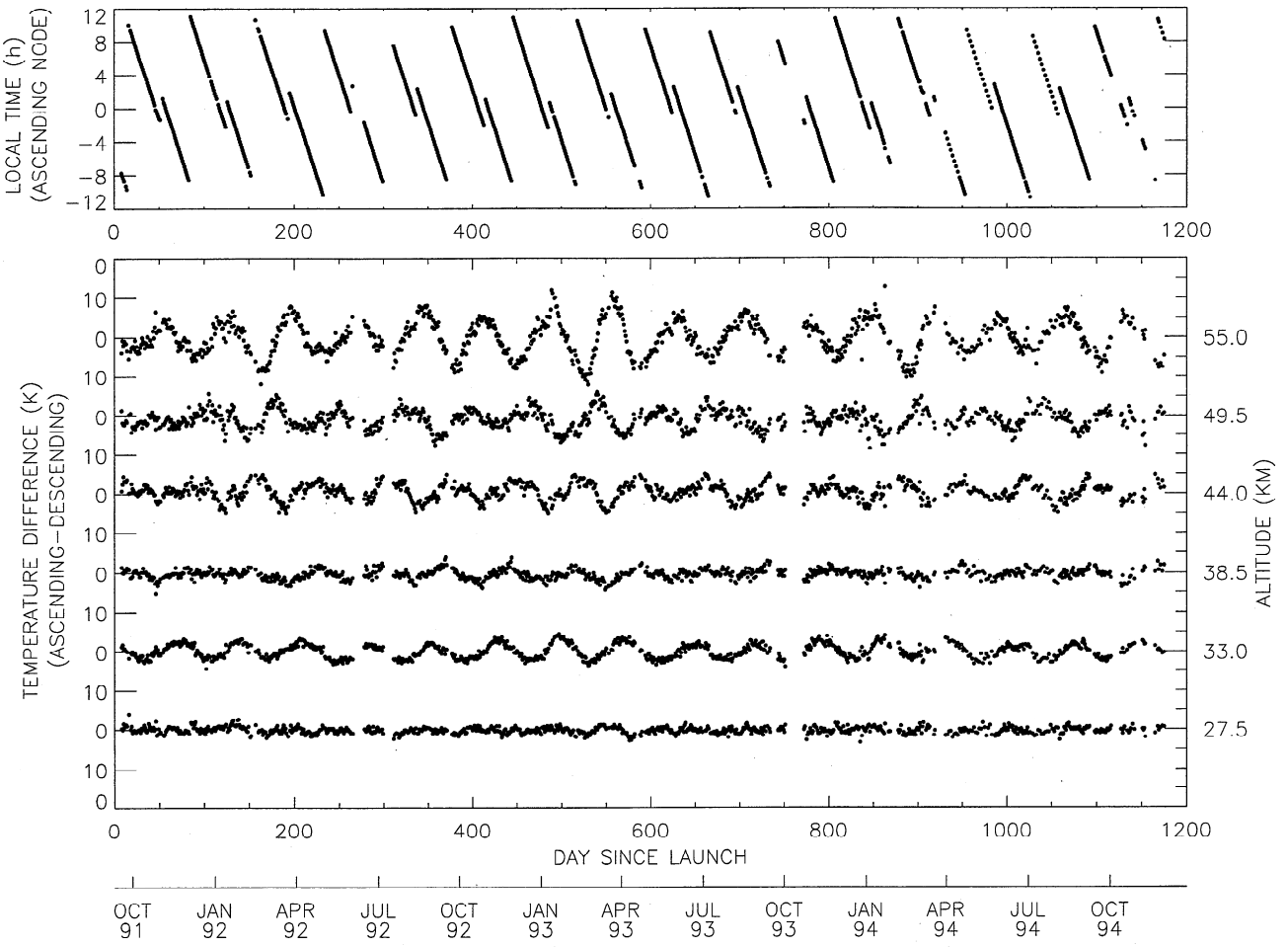

Figure 1. The diurnal tide as a 72-day oscillation in the MLS ascending-descending temperature differences at the equator. The temperature oscillation is generated as the diurnal solar migrating tide is sampled by the ascending and descending nodes that have slightly different local times every day when the UARS orbit precesses. (bottom) Temperature differences at various altitudes. The tick marks on the left are separated by 10 K, while the altitudes are labeled on the right for each time series. (top) Local time of the ascending node.

cause discontinuities (in the tidal variations) which synchronize the UARS yaw period. There are two large data gaps in the period of interest that occurred during October 2–20, 1993, and March 19–28, 1994, while MLS was turned off, which can further degrade the fitting results with an error of ~1 K. The problematic results indeed appear in Figures 2 and 3, which distort the seasonal variation patterns of the tide. The MLS was off every other day for several periods after April 1994, but such a sampling pattern does not significantly reduce the quality of the diurnal tide derived because the gap of the missing data is much shorter than 36 days, the period to cover the diurnal cycle.

4. Diurnal Tide

Figures 2 and 3 show the equatorial diurnal temperature amplitude and phase extracted from MLS A–D temperature differences during 1991–1994. The MLS observations cover the altitude region (28–55 km) where the diurnal tide propagates upward after excitation from the differential heating of upper tropospheric water vapor and latent heat release and starts to interact with the component generated by stratospheric ozone heating. In general, the MLS temperature measurement shows a primarily annual variation of the diurnal tide in the lower stratosphere and a semiannual modulation in the upper stratosphere and mesosphere.

At 22 hPa the annual variation of the diurnal tide yields maximum amplitudes in March at ~15°S and in September at ~15°N. The phases of these maximum amplitudes are locked at ~1600 LT. The seasonal variation is similar for the 3 years including the features at 20°–25°S during November. The amplitude at the equator is very small all the time, giving no indication of the presence of the (1,1) diurnal tide.

At 10 hPa the pattern of the amplitude variation changes remarkably from what is found at the lower altitude (22 hPa). At 5°N the maximum diurnal amplitude (~1.5 K) is observed in February with a phase of ~18 hours. The latitudinal distribution of the diurnal amplitude is similar to that expected for the (1,1) tide but slightly distorted toward the summer hemisphere. The peak tidal amplitude moves around the equator between 5°S and 5°N as the season changes. In August it is located at 5°S with an amplitude of ~1 K and a phase of ~18–20 hours. It is interesting to observe the anticorrelated pattern in the tropical latitudes between the large amplitude at 10 hPa and the small amplitudes at 22 hPa. This anticorrelation may be caused by the interference of the propagating tide with locally excited components.

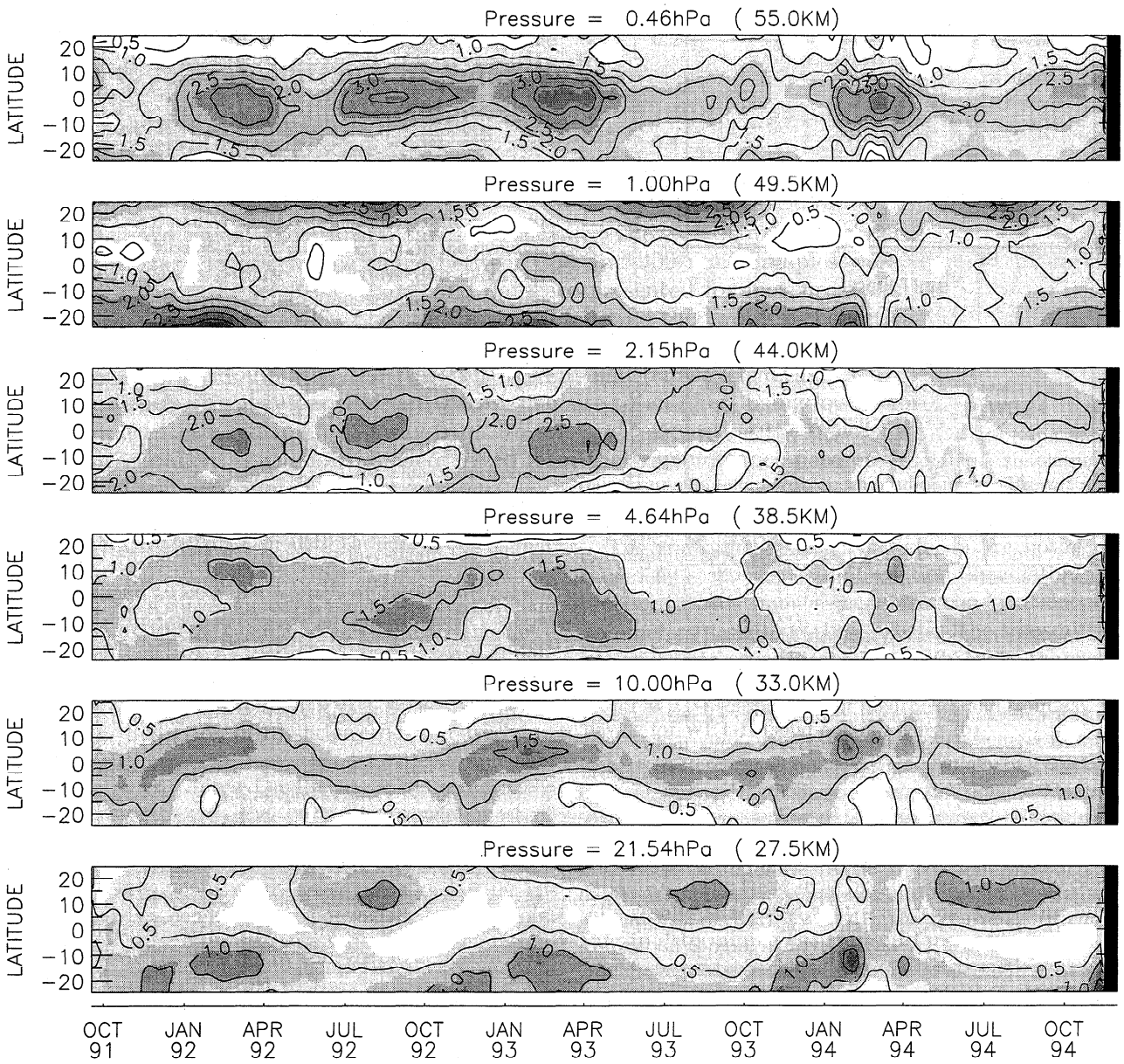

Figure 2. Diurnal temperature amplitudes observed by MLS at pressure levels of 22–0.46 hPa and latitudes of 25°S–25°N. The diurnal tide is extracted from the A–D temperature differences using a least squares fitting method and contoured at an interval of 0.4 K. The discontinuity in March 1994 is caused by a large data gap (see text).

At 4.6–2.2 hPa the diurnal tide in the tropics shows a steady growth in amplitude as it propagates upward from 10 hPa. Its latitudinal structure becomes more symmetric about the equator, as expected for the (1,1) propagating mode. The amplitudes in March and September stand out clearly, producing a strong semiannual variation. In late 1993 and 1994 the diurnal tide almost disappeared, which is correlated very well with the mesospheric quasi-biennial oscillation (MQBO) of the diurnal tide and zonal mean wind [*Burrage et al.*, 1995, 1996].

At 1.0 hPa the tropical diurnal tide is largely depressed, showing no significant seasonal modulations. This may be explained by the interference between the vertically propagating (1,1) tide and the component from local ozone heating that contributes significantly to the propagation and generation of the diurnal tide [*Chapman and Lindzen*, 1970]. The ozone-induced component is quite evident at 20°–25° in the summer hemisphere, characterized by a large diurnal amplitude and a nearly constant phase (~18 hours). The major component of the ozone-induced diurnal tide is in a trapped mode that cannot propagate vertically, but it will interact with the propagating (1,1) mode and cause the depression in the tidal amplitude if the two components are out of phase.

At 0.46 hPa the (1,1) diurnal tide is seen back to its normal growth in amplitude and phase progression and modulated by the same long-term trend as observed at 2.2 hPa. It is characterized by a more symmetric structure at the equator, showing a predominant semiannual variation and stronger amplitudes in 1992–1993 and weaker ones in 1993–1994. The tidal variations seen in MLS temperature are consistent with simultaneous wind observations from UARS high resolution doppler imager (HRDI) in the mesosphere and lower thermosphere [*Burrage et al.*, 1995]. The subtropical features associated with

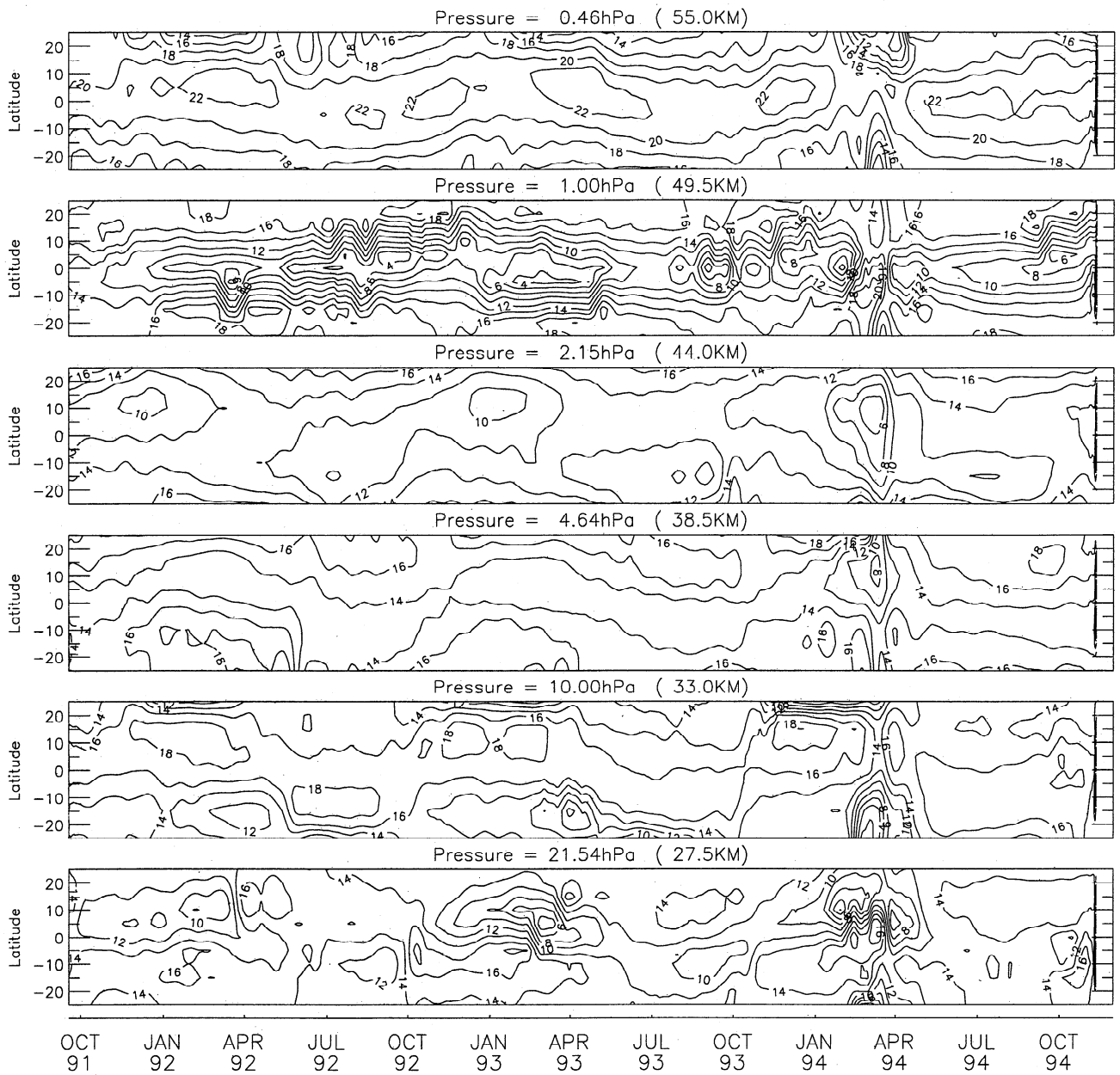

Figure 3. As in Figure 2 but for temperature phases of the diurnal tide. Here phase is defined as the local solar time in hours of the maximum temperature.

ozone heating do not extend to this altitude, which confirms the trapped nature of the ozone-excited diurnal tide. On the other hand, the average amplitudes at 25°S are always higher than those at 25°N over the 3-year period, likely caused by a systematic error in the temperature retrieval.

5. MLS CMAM Comparisons

The Canadian Middle Atmosphere Model (CMAM) is a T32 general circulation model on 50 uneven layers from the surface to ~100 km [*Beagley et al.*, 1998]. The model incorporates the most important heating sources for the diurnal tide such as water vapor and latent heat release due to cumulus convection in the troposphere and ozone in the stratosphere. A parameterization scheme is used to account for orographic gravity wave drag that is critical to mean atmospheric circulations. Since the model outputs are saved every 18 hours in universal time, the diurnal tide is extracted based on four distinct times (0000, 0600, 1200, and 1800 UT).

The diurnal temperature amplitude and phase in the CMAM are extracted using a least squares fitting technique [*McLandress*, 1997] and interpolated to the same pressure-latitude surfaces as in the UARS MLS observations. Figures 4 and 5 show two-year results of the diurnal amplitude and phase simulated by the CMAM. In general, the simulation agrees very well with the MLS observations, reflecting the transition of the tidal variations from annual to semiannual modulations as altitude increases. The long-term tidal variability at 10 hPa is well reproduced, showing the maximum diurnal amplitude at ~10° latitude in the winter hemisphere with a phase of 1800 LT. The model also reveals that the peak latitudes of the diurnal tide and the maximum diurnal heating are not colocated. The diurnal heating rate of water vapor and the latent

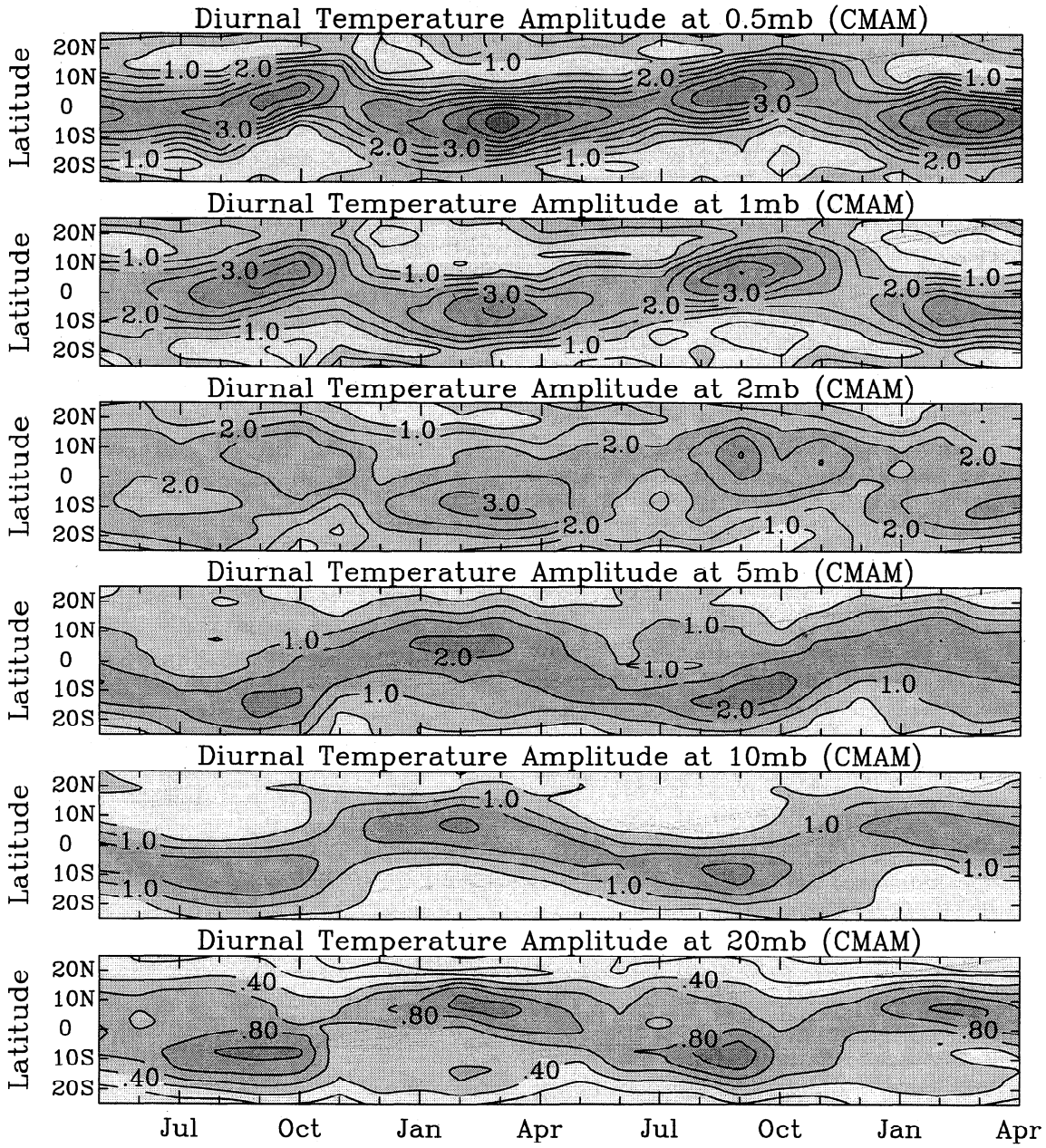

Figure 4. Diurnal temperature amplitudes simulated by the CMAM and labeled at a 0.5 K interval for all the levels except for 20 mbar where a 0.2 K interval is used.

heat release peak at 10°–20° in the summer hemisphere, while the maximum tidal amplitude is in the winter hemisphere at 10 hPa [see *McLandress*, 1997 Figures 10 and 12]. Hence this suggests that the observed tidal structure above 10 hPa is likely influenced more by the background atmospheric conditions than by the upper tropospheric heating.

The tidal features observed at 0.46 hPa are also well reproduced by the CMAM showing the outstanding (1,1) tide in March and September. The CMAM shows temperature amplitudes and mesospheric winds that are comparable to UARS MLS, HRDI, and WINDII observations [*McLandress*, 1997]. *Hagan* [1996], *Burrage et al.* [1995], and *McLandress* [1997] investigated possible causes for the semiannual variation with linear tidal models and concluded that the variability in the heating sources alone cannot explain the strong semiannual modulation of the diurnal tide observed in the mesosphere. Their conclusion is consistent with the MLS temperature observations in the stratosphere not showing any significant semiannual variation until the tide reaches up to 2.2 hPa.

However, some observed features are not produced by the model, most importantly, the tidal seasonal and latitudinal variations at 22 and 1 hPa. At 22 hPa the model simulation is not so different from that at 10 hPa except for somewhat weaker amplitudes, but the MLS observations show an anticorrelated pattern between the two levels in the tropics, which is not seen in the modeled tide at all. In the subtropics the MLS measurement at 22 hPa shows that the maximum tidal amplitude occurs on the summer side of the equator, which also is not reflected in the model simulation. In fact, the subtropical enhancement in the summer hemisphere was observed in the ascending-descending differences of LIMS temperature [*Hitchman and Leovy*, 1985, Figure 1] although this was not

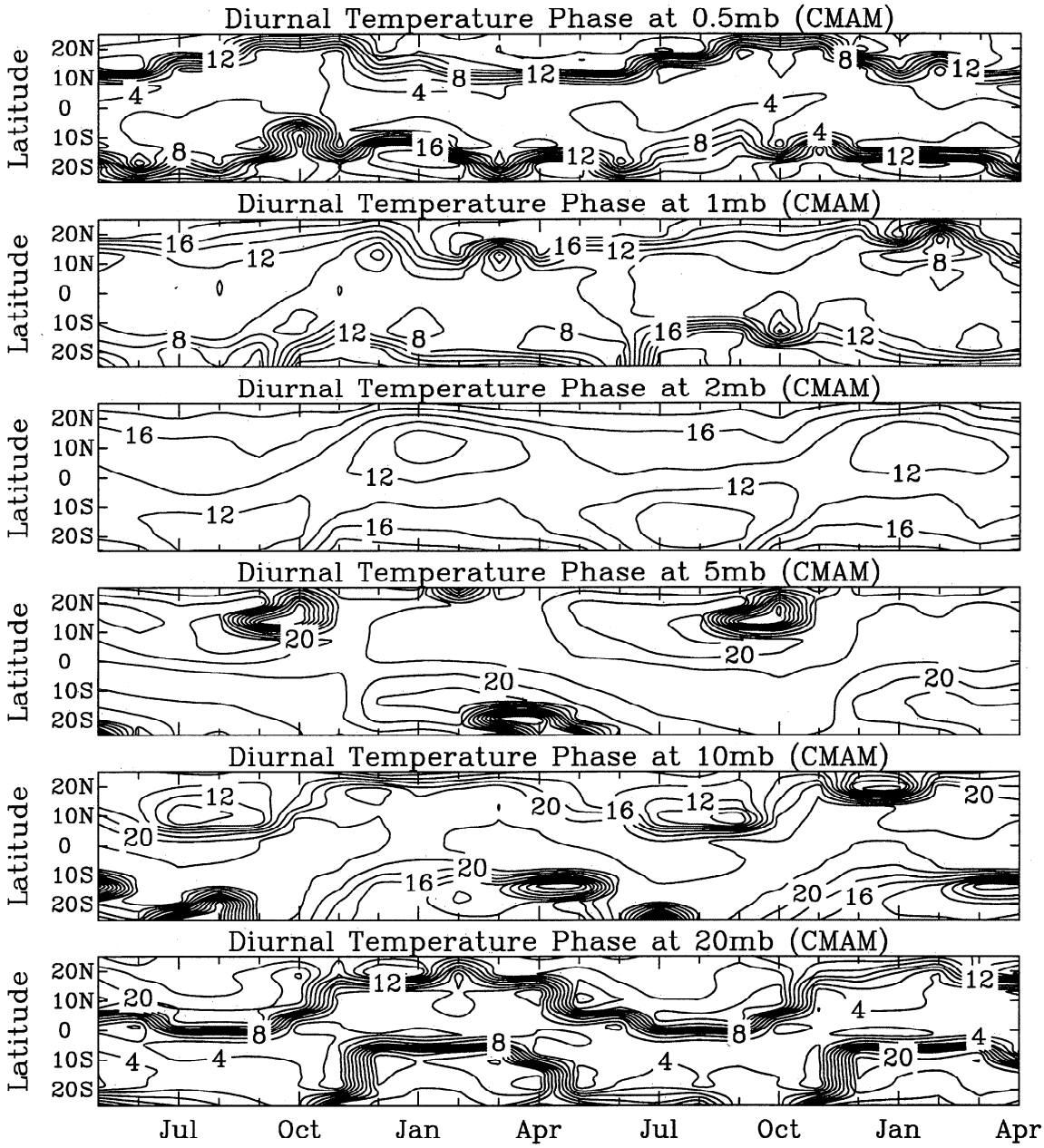

Figure 5. As in Figure 4 but for temperature phases that are contoured at every 4 hours.

discussed by *Hitchman and Leovy* [1985]. They showed that maximum tidal amplitudes occurred in the summer hemisphere at 100 hPa or below and at ~25° latitude, and that the latitudinal structure was incoherent with the (1,1) or other propagating modes above. This latitudinal structure is similar to that of the classical (1, 2) mode, an asymmetric propagating component with a vertical wavelength of 15.5 km, which can be excited by the forcings in the upper troposphere. However, these wave modes can be readily damped in a viscous atmosphere due to their short vertical wavelengths. MLS and limb infrared monitor of the stratosphere (LIMS) temperatures may have observed a piece of these short-lived tidal components that penetrate in the lower stratosphere.

At 1 hPa the CMAM amplitudes at tropical latitudes are much greater than in MLS data, and those at subtropical latitudes do not show the strong annual variation seen by MLS. The discrepancy at 1 hPa may reflect some shortcomings in the CMAM. *McLandress* [1997] showed that the model ozone heating rate for the diurnal tide during solstices has a peak at 1 hPa pressure and maximizes at 20° latitude in the summer hemisphere. However, to yield the pattern observed by MLS at 1 hPa, the maximum ozone heating and the upward propagating (1,1) tide must be out of phase so that the amplitude of the propagating tide is cancelled out at the equator by the ozone heating. In other words, the diurnal tide in the ozone-heating region is very sensitive to the heating profile and the phase of the (1,1) tide, and to obtain the realistic diurnal tide in the middle atmosphere, the CMAM probably needs to further refine its heating/cooling profile.

6. Summary

MLS V4 temperature shows significant improvements from the early version at low altitudes in comparison with NCEP

temperature and yields a useful tidal analysis at 22 hPa. MLS V4 temperature shows smaller biases at 10 and 22 hPa than V3 temperature and agrees better with NCEP in the NH winter (40° poleward) than in the SH winter (40° poleward), suggesting that NCEP temperature may be biased by 3–5 K in the SH due to lack of radiosonde observations.

We have obtained diurnal tidal amplitude and phase at 25°S–25°N for 1991–1994 from MLS ascending-descending temperature differences at 22, 10, 4.6, 2.2, 1, and 0.46 hPa. The diurnal tide observed appears to contain both vertically propagating and trapped components that are combined to show a strong annual variation in the lower stratosphere and a semiannual variation in the upper stratosphere and mesosphere. The signatures of trapped modes are mostly evident at 22 hPa (likely due to excitation in the upper troposphere) and at 1 hPa (due to ozone heating in the stratosphere). The propagating (1,1) mode is a prominent component in the tropics at all other altitudes, showing maximum amplitudes in January–February at 10 hPa and in March and September–October at 2.2 and 0.46 hPa. The large diurnal amplitudes at 10 hPa are well correlated with the small amplitudes at 22 hPa in the long-term time series, likely due to interactions between evanescent and travelling tidal modes. The amplitude of the evanescent mode generated by ozone at 1 hPa is enhanced near solstice and biased toward the summer hemisphere.

The CMAM tidal simulations are in overall good agreement with MLS observations, reproducing many observed features including the annual/semiannual tidal variations in the lower/upper stratosphere. The model tidal amplitude matches the MLS values reasonably well at all levels except at 22 and 1 hPa. The model does not produce a (1, 2) mode-like feature at 22 hPa and the corresponding seasonal variation. The model also gives a too strong tide at tropical latitudes and a too weak tide at subtropical latitudes at 1 hPa.

More studies are required in the future to understand the tidal generation and variation at low altitudes. In order to produce the diurnal tide observed in the lower stratosphere, a numerical model needs realistic diurnal heating rates from water vapor, latent heat release, and other possibly important heating/cooling processes. The diurnal tide study with MLS temperature observations and UARS data can likely help improve the parameterization of these heating profiles.

Acknowledgments. We thank the MLS team for supporting this study, especially Robert Jarnot, Richard Lay, and Dennis Flower for informative discussions on the instrument calibration and operation. This work was performed at the Jet Propulsion Laboratory, California Institute of Technology, under contract with the National Aeronautics and Space Administration (NASA), and sponsored by NASA through the Upper Atmosphere Research Satellite Project.

References

Barath, F.T., et al., The Upper Atmosphere Research Satellite Microwave Limb Sounder instrument, *J. Geophys. Res.*, *98*, 10,751–10,762, 1993.

Beagley, S. R., et al., The radiative-dynamical climatology the first-generation Canadian Middle Atmosphere Model, *Atmos. Ocean*, in press, 1998.

Burrage, M. D., M. E. Hagan, W. R. Skinner, D. L. Wu, and P. B. Hays, Long-term variability in the solar diurnal tide observed by HRDI and simulated by the GSWM, *Geophys. Res. Lett.*, *22*, 2641–2644, 1995.

Burrage, M. D., R. A. Vincent, H. G. Mayr, W. R. Skinner, N. F. Arnold, and P. B. Hays, Long-term variability in the equatorial middle atmosphere zonal wind, *J. Geophys. Res.*, *101*, 12,847–12,854, 1996.

Chapman, S., and R. S. Lindzen, *Atmospheric Tides*, Gordon and Breach, Newark, N.J., 1970.

Fishbein, E. F., et al., Validation of UARS Microwave Limb Sounder temperature and pressure measurements, *J. Geophys. Res.*, *101*, 9983–10,016, 1996.

Fleming, E. F., et al., Monthly mean global climatology of temperature, wind, geopotential height and pressure from 0–120 km, *NASA Tech. Memo.*, *TM-100697*, 85 pp., 1988.

Forbes, J. M., and H. B. Garrett, Theoretical studies of atmospheric tides, *Rev. Geophys.*, *17*, 1951–1981, 1979.

Fritts, D. C., and R. A. Vincent, Mesospheric momentum flux studies at Adelaide, Australia: Observations and gravity wave/tidal interaction model, *J. Atmos. Sci.*, *44*, 605–619, 1987.

Hagan, M. E., Comparative effects of migrating solar sources on tidal signatures in the middle and upper-atmosphere, *J. Geophys. Res.*, *101*, 21,213–21,222, 1996.

Hays, P. B., and D. L. Wu, and HRDI Team, Observations of the diurnal tide from space, *J. Atmos. Sci.*, *51*, 3077–3093, 1994.

Hitchman, M. H., and C. B. Leovy, Diurnal tide in the equatorial middle atmosphere as seen in LIMS temperatures, *J. Atmos. Sci.*, *42*, 557–561, 1985.

Lindzen, R. S., Turbulence and stress owing to gravity wave and tidal breakdown, *J. Geophys. Res.*, *86*, 9707–9714, 1981.

Manney, G. L., et al., Comparison of U.K. Meteorological Office and U.S. National Meteorological Center stratospheric analyses during northern and southern winter, *J. Geophys. Res.*, *101*, 10,311–10,334, 1996.

Manson, A. H., C. E. Meek, M. J. Smith, and G. J. Fraser, Direct comparison of prevailing winds and tidal wind fields (24-, 12-h) in the upper middle atmosphere (60–105 km) during 1978–1980 at Saskatoon (52°N, 107°W) and Christchurch (44°S, 173°E), *J. Atmos. Terr. Phys.*, *47*, 463–476, 1985.

McLandress, C., Seasonal variability of the diurnal tide: Results from the Canadian middle atmosphere general circulation model, *J. Geophys. Res.*, *102*, 27,747–27,764, 1997.

McLandress, C., et al., The meridional wind component of the thermospheric tide observed by WINDII on UARS, *Geophys. Res. Lett.*, *21*, 2417–2420, 1994.

McLandress, C., G. G. Shepherd, and B. H. Solheim, Satellite observations of thermospheric tides: Results from the Wind Imaging Interferometer on UARS, *J. Geophys. Res.*, *101*, 4093–4114, 1996.

Reed, R. J., M. J. Oard, and M. Sieminski, A comparison of observed and theoretical diurnal tidal motions between 30 and 60 kilometers, *Mon. Weather Rev.*, *97*, 456–459, 1969.

Vial, F., Numerical simulations of atmospheric tides for solstice conditions, *J. Geophys. Res.*, *91*, 8955–8969, 1986.

Vial, F., J. M. Forbes, and S. Miyahara, Some transient aspects of tidal propagation, *J. Geophys. Res.*, *96*, 1215–1224, 1991.

Vincent, R. A., T. Tsuda, and S. Kato, Asymmetries in mesospheric tidal structure, *J. Atmos. Terr. Phys.*, *51*, 609–616, 1989.

Walterscheid, R. L., Inertio-gravity wave induced accelerations of mean flow having an imposed periodic component: Implications for tidal observations in the meteor region, *J. Geophys. Res.*, *86*, 9698–9706, 1981.

Waters, J. W., Microwave limb sounding, in *Atmospheric Remote Sensing Microwave Radiometry*, edited by M. A. Janssen, pp. 383–496, John Wiley, New York, 1993.

Wu, D. L., P. B. Hays, and R. G. Roble, Doppler imager wind measurements with simulations from the NCAR thermosphere-ionosphere-mesosphere electrodynamics circulation model, *J. Geophys. Res.*, *101*, 19,147–19,160, 1996.

L. Froidevaux, W. G. Read, J. W. Waters, and D. L. Wu, Jet Propulsion Laboratory, California Institute of Technology, MS 183-701, 4800 Oak Grove Dr., Pasadena, CA 91109. (e-mail: dwu@mls.jpl.nasa.gov)

C. McLandress, Department of Atmospheric Science, University of Washington, Box 351640, Seattle, WA 98195. (e-mail: charles@atmos.washington.edu)

(Received October 27, 1997; revised January 28, 1998; accepted February 5, 1998.)